

RELATIONSHIP OF THE MULTIMODE KINK INSTABILITY TO δ -SPOT FORMATION

M. G. LINTON,¹ G. H. FISHER,¹ R. B. DAHLBURG,² AND Y. FAN³
Space Sciences Laboratory, University of California, Berkeley, Berkeley, CA 94720

Received 1998 November 20; accepted 1999 April 20

ABSTRACT

We study the current-driven kink instability with a three-dimensional MHD spectral code, under conditions appropriate for the convection zone of the Sun. Our goal is to determine whether the kink instability can explain the unusual morphology of certain “ δ -spot” active regions. The characteristics of these δ -spots are unusually large tilt upon emergence, subsequent rotation, compactness during their lifetime, magnetic shear that develops along the neutral line of their vertical magnetic field, and unusually high flare activity. We find that highly twisted tubes perturbed with a single unstable kink mode evolve to a new helical equilibrium with finite amplitude. This kink would produce an active region that emerged tilted and then rotated and so is suggestive of δ -spot behavior. It would not, however, produce other characteristics of δ -spots such as compactness and shear. We then investigate the kink instability in tubes perturbed simultaneously with several unstable modes at different wavelengths. These tubes develop a concentrated kink at the point at which the modes interact constructively. We show that such a concentrated kink would first emerge highly tilted, rotate during its subsequent emergence while remaining compact, and develop strong shear along its magnetic neutral line, in agreement with δ -spot observations. In addition we find that very strong concentrated kinks develop a current sheet at which the magnetic field reconnects, causing field lines near the center of the tube to become knotted. This reconnection could be related to the high flare activity of δ -spots.

Subject headings: MHD — Sun: activity — Sun: interior — Sun: magnetic fields — sunspots

1. INTRODUCTION

Sunspots are concentrations of magnetic field observed in the photosphere of the Sun. They are typically tens of thousands of kilometers in diameter and consist of a dark region, or umbra, with magnetic field of several kilogauss surrounded by a brighter penumbra of somewhat lower magnetic field. Both the umbra and penumbra are darker in white light than the quiet photosphere, and the field strengths in the umbra and penumbra are typically 2 orders of magnitude higher than the average field strengths in the quiet photosphere. Sunspots often emerge into the photosphere as small pairs of opposite magnetic polarity spots that grow over the course of several days into a full-sized sunspot group. A fully developed spot group typically consists of one or more “leading” polarity spots, with several “following” spots of the opposite polarity trailing behind, in that sense of the Sun’s rotation. Together with the coronal magnetic loops that connect them and other associated magnetic features, these are called “active regions.”

It is well known observationally that the magnetic axis of most active regions remains only slightly tilted ($\sim 6^\circ$) toward the equator, with the leading spots lying closer to the equator. In addition, for a given solar cycle and a given hemisphere (north or south), the polarity of the leading portion of the spot group tends to be the same for most active regions, as first noted by Hale et al. (1919) and as laid out in the so-called Hale-Nicholson law. The special class of active regions called δ -spot active regions are an exception to these rules. These are active regions in which sunspot umbrae of opposite polarity exist within the same penum-

bra (Künzel 1960) and are therefore much more compact than normal active regions. They are often highly tilted away from the east-west orientation, sometimes so much that they have an inverse Hale-Nicholson configuration, and their magnetic field is often sheared along the magnetic neutral line at the juxtaposition of the two opposite polarity spot groups (Zirin & Liggett 1987; Lites et al. 1995). In addition they are often observed to rotate about one another as they evolve (Leka et al. 1996; Tanaka 1991). These active regions are of particular interest because they are known to be much more flare active than normal active regions. For example, Tanaka (1980) found that 90% of the δ -spots with inverted polarity he studied had flare activity, and Sammis & Zirin (1998) studied a set of 18,215 *GOES* flares and found that 50 of 64 regions for which X1 or larger flares occurred were δ -spot regions.

In this paper we study a possible mechanism, the current driven kink instability, for the formation of “island δ -spots,” that is, regions that emerge as δ -spots rather than being created from the collision of previously emerged umbrae.

An active region is believed to be the manifestation in and above the photosphere of the apex of a magnetic flux tube that arches into the corona from the convection zone. The two opposite polarities of a bipolar active region are created by the intersection with the photosphere of the two legs of this arched flux tube. The fact that the two polarities are made up of a number of separate spots is likely due to the fact that the emerged portion of the flux tube has fragmented. As the flux tube first emerges, a normal active region appears as two close, small regions of opposite polarity. As the tube emerges further, the spots coalesce and grow until they encompass the whole cross section of tube, and the magnetic polarities separate as more of the arch emerges into the corona. The usual explanation for the Hale-Nicholson law is that the source of the flux tubes, likely to be at the base of the convection zone, consists of a

¹ Space Sciences Laboratory, University of California, Berkeley, CA 94720.

² Laboratory for Computational Physics and Fluid Dynamics, Naval Research Laboratory, Washington, DC 20375-5344.

³ High Altitude Observatory, National Center for Atmospheric Research, PO Box 3000, Boulder, CO 80307.

magnetic field parallel to the equator that breaks off into flux tubes and rises to the surface, with the flux tubes keeping approximately the same orientation parallel to the equator during their rise and emergence.

The morphology of δ -spots suggests that the flux tubes that create these active regions have undergone some change during their rise so that they do not evolve as normal spot groups do. These tubes have been distorted so that their apex does not emerge parallel to the equator and so that the sunspot pairs they create do not separate as the tube emerges, resulting in a rotated, compact active region. This, together with observations of δ -spots rotating during their evolution, indicates that the legs, rather than forming a simple arch, are wrapped or knotted around each other. In Linton et al. (1998) we studied the kink instability, which distorts magnetic flux tubes with twisted field lines into a helical shape, as a potential source for these unusual δ -spot configurations. We found the kink distorts the tubes studied into a helical equilibrium with amplitude large enough to generate moderate tilt in an active region. Our goal in this paper is to continue our study of the kink instability as it applies to rising convection zone flux tubes and to continue exploring how the emergence of a kinked flux tube relates to the formation and evolution of a δ -spot active region. We review the kink instability in § 2 and discuss the nonlinear code we use to simulate the instability in § 3. We present our numerical results, where we find that concentrated kinks can develop on sufficiently twisted flux tubes, in § 4. We present our conclusions about the evolution of a rising, kinking convection zone flux tube and compare these conclusions with the simulations of Fan et al. (1999) in § 5. Then we discuss the implications of these results, namely that concentrated kinks can create spot regions that strongly resemble δ -spot active regions, and we discuss the predictions these results imply about the sense of δ -spot rotation relative to the sense of magnetic twist in § 6.

2. REVIEW OF THE KINK INSTABILITY

The current-driven kink instability was first proposed by Alfvén (1950) as a dynamo mechanism, in analogy with the observed kink instability in twisted wires. It occurs in tubes in which the field lines are highly twisted and converts field line twist into helical deformations of the tube axis, or “writhe” (Moffatt & Ricca 1992), to reduce the magnetic energy (see § 5.4 of Linton et al. 1998). A flux tube’s susceptibility to the kink instability depends on the interplay of the stabilizing axial field tension, which works to keep the tube straight, and the destabilizing azimuthal field pressure force, which acts to bend the tube (see Kruskal & Schwarzschild 1954). The linear stability of various flux tube profiles has been widely studied in both nuclear fusion (see, e.g., Shafranov 1957; Suydam 1959) and solar applications (see review in Priest 1982, p. 259; and Linton, Longcope, & Fisher 1996), and it has been well established that the ratio of the azimuthal to axial field is the key measure of the kink instability of a tube. Tubes with magnetic field $B(x) = [0, B_\theta(r), B_z(r)]$ in cylindrical coordinates become kink unstable when the twist

$$q \equiv \frac{B_\theta}{rB_z} \quad (1)$$

becomes larger than some critical value q_{cr} .

In Linton et al. (1996), we studied the linear instability of uniform-twist [$q(r) = \text{constant}$] infinitely long flux tubes to kink perturbations of the form $\xi(r)e^{i(kz+\theta)+\omega t}$, where ξ is the displacement eigenfunction, and ω is the growth rate eigenvalue. The critical twist for instability is well approximated by $q_{cr} = a^{1/2}$, where a is a measure of the radial profile of the axial field, taken from the Taylor series expansion: $B_z(r) = B_0(1 - ar^2 + \dots)$. The tubes are unstable to a finite range of wavenumbers k centered about $k = -q$. The fact that k and q have opposite signs has the important implication that the helical sense of the kink (right- or left-handed) is determined by the sign of the twist. In the small twist limit, $q^2 \ll R^{-2}$, where R is the external tube radius, the limits of the unstable wavenumber range can be written as $k/q = -1 \pm \Pi$, and both Π and the maximum growth rate ω_{max} scale as

$$\Pi \propto \frac{\omega_{max} R}{v_A} \propto R^2(q^2 - q_{cr}^2). \quad (2)$$

Here the growth rate has been normalized by the tube Alfvén crossing time R/v_A , where the Alfvén speed is given by $v_A^2 = B_0/(4\pi\rho_0)$ and B_0 and ρ_0 are the magnetic field strength and density on the tube axis. We plot several dispersion relations in Figure 1, calculated as in Linton et al. (1996), for highly twisted tubes with field profiles given by what we will call an “ α -profile:”

$$B_z = B_0 \left(1 - \frac{r^2}{R^2}\right)^\alpha, \quad B_\theta = qrB_z, \quad (3)$$

for $r < R$, and $B = 0$ for $r > R$. The magnetic forces in these non-force-free configurations are balanced by radial pressure gradients. The magnetic profiles for the curves labeled A through D have $\alpha = 0.25$ and have normalized twist qR

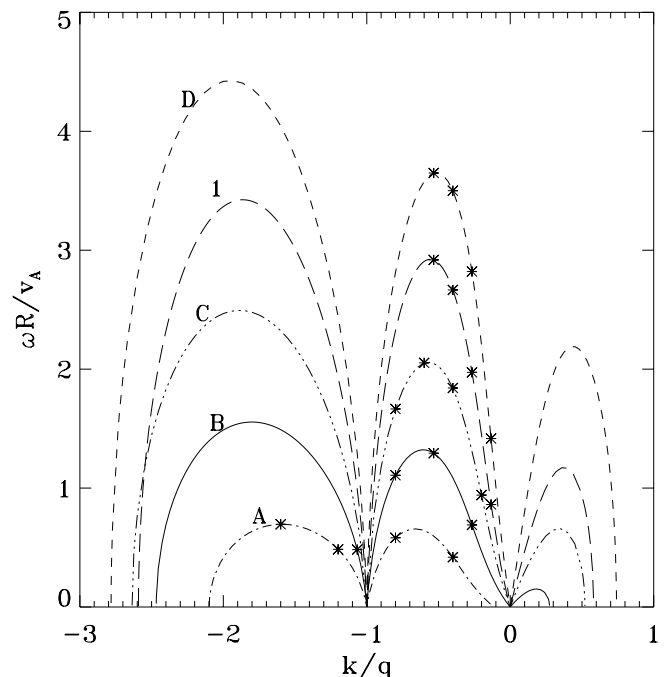


FIG. 1.—Dispersion relations for five α -profile flux tubes (eq. [3]). Curves A, B, C, and D are for $\alpha = 0.25$ with $qR = 1.96, 2.95, 3.93,$ and 5.89 , respectively. The curve marked 1 is for $\alpha = 1$ with $qR = 5.89$. The four modes $n = 1, 2, 3,$ and 4 are marked on each curve with asterisks.

varying from 1.96 to 5.89. The curve labeled 1 is for an $\alpha = 1$, $qR = 5.89$ profile. A Taylor series expansion of the axial field in equation (3) shows that the r^2 coefficient a equals α/R^2 , so the critical twist is $q_{\text{cr}} = \alpha^{1/2}/R$. For these profiles $q^2 R^2 \gg q_{\text{cr}}^2 R^2 = \alpha$, so $\omega_{\text{max}} R/v_A$ should vary as $q^2 R^2$ if the weak twist results can be extended to this range of twist. In fact, for a variation in $q^2 R^2$ of a factor of 9 for the $\alpha = 0.25$ tubes in Figure 1, $\omega_{\text{max}} R/v_A$ varies by a factor of 6.4, so while relation (2) does not hold exactly, it is a reasonable approximation. Note that this has a very important implication if the tube expands homologously as it rises through the convection zone, meaning that the field profile scales so that only the values of R and B_0 change in equation (3). As the tube expands, the profile A ($qR = 1.96$) tube will eventually evolve to a profile D ($qR = 5.89$) tube, and its dispersion relation will evolve accordingly. Thus simply by expanding, tube A will become more kink unstable. For tubes with subcritical twist, this effect will be even more dramatic: the critical twist q_{cr} for homologously expanding tubes scales as $1/R$ (e.g., $q_{\text{cr}} = \alpha^{1/2}/R$ for eq. [3]) while the twist q remains constant (see Linton et al. 1996, § 5), meaning that tubes that are initially kink stable can become unstable as they rise. This increased kink instability due to expansion can be explained by noting that, assuming magnetic flux conservation and homologous expansion, B_z decreases as $1/R^2$, while B_θ only decreases as $1/R$.

Note that for highly twisted tubes the unstable range in k space also expands approximately as predicted by relation (2) and therefore eventually extends to $k \geq 0$. The tube is stable at $k = 0$, and the instability is weakened as k approaches zero, but for sufficiently highly twisted tubes instability does appear for positive k values. For the $\alpha = 0.25$ tube profiles shown in Figure 1 we find that positive- k unstable modes appear for $qR \geq 2.24$. We will discuss these modes again briefly in § 4.1, but as they only appear at very high twist, long after negative- k modes have become unstable, we do not investigate their nonlinear evolution in this paper.

The marginally stable point at $k/q = -1$ occurs when the kink pitch exactly equals the field line pitch, meaning the kink is in resonance with the field lines and the tube is marginally stable. This resonance phenomenon is important in non-uniform-twist tubes. The marginally stable point in the dispersion relation then manifests itself as a marginally stable surface in the tube, called the mode resonant surface, where the local twist exactly equals the wavenumber of the kink. In this case, the kink is an ‘‘internal kink’’ that occurs within this cylindrical surface, initially leaving the tube outside the surface undisturbed. The nonlinear evolution of the internal kink has been extensively studied in two and three dimensions in the tokamak literature (see Waddell et al. 1976 or Sykes & Wesson 1976 for early results). These studies find that the helical deformation of the kink pushes the tube into the mode resonant surface, where a current sheet develops. The flux inside the mode resonant surface, where $q > |k|$, then reconnects at the current sheet with flux outside the surface, where $q < |k|$ (see, e.g., Aydemir, Wiley, & Ross 1989; Baty 1997), effectively smoothing out the twist profile and earning this instability the name ‘‘resistive kink.’’ The reconnected flux tube then returns to a cylindrical configuration with essentially uniform twist (see, e.g., Waddell et al. 1976; Aydemir et al. 1989; or Fig. 7d of Vlad & Bondeson 1989). In the convection zone, it is possible that these internal or resistive kinks

will be suppressed by the low resistivity of the convection zone. If they do occur, however, we expect that they will cause cylindrically symmetric twisted flux tubes with non-uniform-twist profiles to tend toward cylindrically symmetric uniform-twist tubes, as in equation (3). In either case, the tubes will then be unstable to the external kink, which we study here with uniform-twist tubes. As shown in Linton et al. (1998), these externally kinked tubes will evolve to a kinked equilibrium and will thus preserve evidence of the kink as the tube rises to the photosphere.

Recently it has become possible to simulate the kink instability in three dimensions numerically (see, e.g., Galsgaard & Nordlund 1997; Matsumoto et al. 1998; Lionello et al. 1998; Fan et al. 1998b, 1999; and Linton et al. 1998, 1999). In Linton et al. (1998), we studied the nonlinear evolution of the kink for a number of different flux tubes with a range of twist values and axial field profiles. We numerically simulated single-mode (wavelength) instabilities in twisted tubes embedded in a high plasma- β environment, meant to represent convection zone conditions. We focused on modes near the peak of the dispersion relation, $\omega \sim \omega_{\text{max}}$, arguing that modes with the highest growth rate were the best candidates for producing large kinks. The growth rates of the kinks studied agreed very well with those predicted by the linear theory in Linton et al. (1996) (see Linton et al. 1998), and the kinks stopped evolving and reached new equilibria in about 10 linear growth times, indicating that tubes will have sufficient time to kink during their rise through the convection zone. The tubes evolved to right-handed helical equilibria for these right-hand twisted tubes, as predicted, with amplitudes of up to $R/3$. We concluded that such a helical flux tube would generate a spot region which would emerge tilted away from the east-west direction and then rotate, as a δ -spot does. The fact that right- (left-) hand twisted tubes develop right- (left-) hand twisted kinks allows us, if the sign of the twist is known, to predict the sense of both the initial tilt and rotation that an emerging kinked region would have (see discussion in § 6). Our goal here is to extend our study of the kink instability to other regions of k -space. We simulate kinks at longer wavelengths and then simulate the interaction of multiple kink modes in a tube. We then study how this affects the kink amplitude and morphology and how this relates to δ -spot characteristics. We present results of the single-mode simulations at long wavelengths in § 4.1, results of the multiple-mode simulations in § 4.2, and results of multiple mode simulations for tubes with differing amounts of twist in § 4.3.

3. SIMULATIONS

We performed three-dimensional magnetohydrodynamic simulations of the kink instability using a visco-resistive, periodic, spectral code on a 128^3 grid. The governing equations for this compressible MHD system are (as adapted from Dahlburg, Antiochos, & Norton 1997)

$$\frac{\partial \rho}{\partial t} = -\nabla \cdot (\rho \mathbf{v}), \quad (4)$$

$$\rho \frac{D\mathbf{v}}{Dt} = \frac{\mathbf{J} \times \mathbf{B}}{c} - \nabla p + \mu \nabla \cdot \boldsymbol{\tau}, \quad (5)$$

$$\frac{\partial \mathbf{B}}{\partial t} = \nabla \times (\mathbf{v} \times \mathbf{B}) + \eta \nabla^2 \mathbf{B}, \quad (6)$$

$$\frac{\partial U}{\partial t} = -\nabla \cdot (U\mathbf{v}) - p\nabla \cdot \mathbf{v} + \mu\boldsymbol{\tau} \cdot \nabla\mathbf{v} + \kappa\nabla^2 T + \frac{4\pi\eta}{c^2} |\mathbf{J}|^2, \quad (7)$$

$$p = \rho RT = (\gamma - 1)U, \quad (8)$$

$$\nabla \cdot \mathbf{B} = 0. \quad (9)$$

Here $\mathbf{v}(x, t)$ is the flow velocity, $p(x, t)$ is the plasma pressure, $T(x, t)$ is the temperature, $U(x, t)$ is the internal energy density, $\mathbf{J} \equiv (c/4\pi)\nabla \times \mathbf{B}$ is the current, $\tau_{i,j}(x, t)$ is the viscous stress tensor, R is the ideal gas constant, $\gamma = 5/3$ is the adiabatic ratio, and c is the speed of light. Uniform thermal conductivity (κ), magnetic resistivity (η), and viscosity (μ) are assumed, with a viscous Lundquist number $S_v \equiv \rho_0 v_A R/\mu$ of 120, a resistive Lundquist number $S_r \equiv v_A R/\eta$ of 1.2×10^5 , and $\beta \equiv 8\pi p_0/B_0^2$ of 600. In these definitions, p_0 is the initial pressure at the center of the flux tube. For a 10^{21} Mx, 10^5 G flux tube at the base of the convection zone, we estimate the actual values of these dimensionless numbers to be $S_v = 10^{12}$, $S_r = 10^{10}$, and $\beta = 10^5$, where the resistivity is taken from Stix (1989, p. 253), the viscosity is taken from Priest (1982, p. 81), and the values of the pressure, temperature, and density are taken from Table 6.1 of Stix (1989). For most runs, the magnetic field is given by equation (3) with a ratio of tube radius R to the tube length L of 1/8. As this is not a force-free configuration, the initial equilibrium is created by setting the plasma pressure profile so that the pressure gradient balances the magnetic forces. For more details on the code, which was run on the Naval Research Laboratory's CM500e, see Dahlburg et al. (1997).

At the start of each run, we perturb the equilibrium profile with one or more helical velocity profiles [$\mathbf{v}(x) = v_0 \boldsymbol{\xi}(r)e^{i(\theta + kz)}$], where $\boldsymbol{\xi}(r)$ is the linear kink eigenfunction calculated as in § 2 of Linton et al. (1996), and the amplitude v_0 is set to $v_A/140$. The wavenumber k is chosen so that the tube is kink unstable according to linear stability calculations (see Fig. 1). The multimode simulations are given initial perturbations consisting of the superposition of these velocity profiles for several unstable k values.

In addition to the α -profile tubes, we also simulated one constant-twist tube where B_z had a Gaussian profile: $B_z = B_0 \exp(-r^2/R_0^2)$, $B_\theta = qrB_z$. This allowed us to compare our code to the anelastic MHD code used by Fan et al. (1998b, 1999) for an identical simulation. As was the case for the other tubes, the field was set to zero outside a finite radius, $r/L = 5/16$, where L was the tube length. We set R_0/L to $5/64$, and qR_0 to 4. The instability was excited by giving the tube a helical velocity perturbation of wavenumber $k = -6\pi/L$.

The anelastic code of Fan et al. (1998b, 1999) filters out sound waves and is suitable for studying slow, subsonic dynamic processes in a gravitationally stratified layer of high- β plasma (see, e.g., Gilman & Glatzmaier 1981). The main advantage of the anelastic code is that it can take into account the effects of gravity and stratification, which our periodic code cannot, and can therefore accommodate a kink-unstable flux tube as it rises and expands in a convection zone-like environment. On the other hand, our code solves the fully compressible MHD equations and is less dissipative ($v_A R_0/\eta = 75,000$) than Fan et al.'s code ($v_A R_0/\eta = 4300$). For this run, the gravity was turned off in Fan et al.'s code, and the resistivities in both codes were changed to $v_A R_0/\eta = 15,000$, so that the two simulations could be compared. As the kink we are simulating is ideal

and incompressible in the linear limit, the evolution should be nearly identical in the two simulations. However, if the presence of sound waves becomes important in the nonlinear stages of the kink evolution, we might expect to see a difference between the two simulations. We found good qualitative agreement between the two codes for the linear and nonlinear kinetic energy evolution and the final equilibrium time of the kinked tube. We measured the linear e-folding time of the instability and found a time of $0.38R_{\text{rms}}/v_A$ for Fan et al.'s code and a time of $0.39R_{\text{rms}}/v_A$ for our code, a difference of less than 3%. We also found that the overall behavior of the tube was the same as that of an α -profile tube.

4. RESULTS

4.1. Single-Mode Kinks

In Linton et al. (1998) we performed a number of simulations in which we perturbed a twisted equilibrium tube with a single unstable kink mode lying near the peak of the tube's dispersion relation. We measured the amplitude of the displacement Δx of the field weighted center of mass of the tube,

$$\Delta x \equiv \left| \frac{\int dA |\mathbf{B}| x}{\int dA |\mathbf{B}|} \right|, \quad (10)$$

where the integral is taken over a plane perpendicular to the initial tube axis. Taking the y - z plane to be parallel to the plane of the photosphere, the displacement of the tube relative to the \hat{z} axis, or the east-west direction, will be

$$y = \Delta x \sin(kz). \quad (11)$$

This then gives a maximum tilt ϕ for the kinked tube that satisfies

$$\tan \phi \equiv \left. \frac{dy}{dz} \right|_{y=0} = k \Delta x. \quad (12)$$

We found a maximum displacement for the modes studied of $\Delta x \sim R/3$ and a corresponding maximum tilt angle of $\phi \sim 30^\circ$. In addition, we found that, while a variation in q or α gave the predicted variation in the linear growth rate of the kink, it did not have a noticeable effect on Δx (see Fig. 9 of Linton et al. 1998). We now extend these single-mode kink simulations of Linton et al. (1998) to include modes that lie away from the peak of the dispersion relation. We simulate an α -profile tube for $\alpha = 0.25$ and $qR = 5.89$ in four single mode simulations at $n = 1, 2, 3$, and 4, where $n \equiv -kL/2\pi$ (see runs 1–4 in Table 1). The dispersion relation for this tube is shown in Figure 1 as the dashed line labeled D, and these four modes are indicated on that curve with the asterisks. Magnetic field isosurfaces of the resulting kinked tubes are shown in Figure 2, from which one can see that the amplitude of the kink increases dramatically as n decreases from 4 to 1. The displacements and corresponding tilt angles for these kinks are shown in Table 1. The $n = 1$ kink in particular has a very large displacement Δx of almost $2R$.

We calculated the magnetic energy released as the difference between the initial (E_{B0}) and final (E_{Bf}) integral of the magnetic energy density over the whole simulation volume, where

$$E_B \equiv \int d^3x \frac{B^2}{8\pi}. \quad (13)$$

TABLE 1
INITIAL AND KINKED TUBE PARAMETERS

Run	Profile	qR	$q_{cr}R$	n	E_r/E_0	Λ_0	Λ	$\Delta x/R$	ϕ
1	D	5.89	0.5	1	0.33	3.5	0.83	1.9	56
2	D	5.89	0.5	2	0.45	3.5	0.66	0.67	47
3	D	5.89	0.5	3	0.49	3.5	0.45	0.33	38
4	D	5.89	0.5	4	0.50	3.5	0.23	0.16	27
5	D	5.89	0.5	1, 5	0.5	3.5	0.15
6	D	5.89	0.5	3, 4	0.5	3.5	0.27
7	D	5.89	0.5	1-4	0.52	3.5	0.17
8	D	5.89	0.5	1-7	0.52	3.5	0.23
9	A	1.96	0.5	1-4	0.13	1.2	0.25
10	B	2.95	0.5	1-4	0.23	1.8	0.39
11	C	3.93	0.5	1-4	0.36	2.3	.21
12	I	5.89	1.	1-4	0.34	1.8	0.18

NOTE.—The profiles correspond to the labels in Fig. 1. These are given by eq. (3), where q is the twist, and $\alpha = 0.25$ for all but profile 1, for which $\alpha = 1$. The critical twist is calculated as $q_{cr} = \alpha^{1/2}/R$, where R is the external tube radius. $n = -kL/2\pi$, where k is the wavenumber of the kink, and L is the length of the tube. The ratio E_r/E_0 is the magnetic energy released during the kink over the initial magnetic energy. The global force-free parameter Λ is defined in eq. (30): Λ_0 is the initial value, and Λ is the final value. The helical kink displacement Δx is calculated as in eq. (10), and the tilt angle ϕ this produces is calculated in eq. (12). These two parameters are calculated only for the four single-mode kinks, as they are poorly defined for multiple-mode kinks.

The plot of this energy release versus mode number in Figure 3a, where the single-mode kinks are plotted as asterisks, shows that this displacement is not energetically favorable: the energy released by the kink decreases with decreasing n . The $n = 2, 3$, and 4 kinks appear to have released sufficient magnetic energy, about 50% of the initial magnetic energy, to have reached an equilibrium state, but as we will discuss below, the $n = 1$ kink has not.

The kink involves a stretching of the tube, a writhing of the tube into a helical shape, and motions within the tube. The tube is stretched because the new helical axis of the tube is longer than the initial, straight axis, and the effect of this stretching on the total magnetic energy can be estimated in a straightforward fashion with the following schematic analysis. Although this analysis does not represent the entire effect of the kink, we present it to give some insight into what is happening.

Assume the tube starts out cylindrically symmetric with axis $\hat{l} = \hat{z}$, area πR^2 , and length L . When it kinks to a helical configuration with wavenumber k and axial displacement Δx , the axis becomes $\hat{l} = (\hat{z} + k \Delta x \hat{\theta})/\kappa$, where

$$\kappa \equiv \sqrt{1 + k^2 \Delta x^2}. \tag{14}$$

The axial length becomes

$$L = \kappa L, \tag{15}$$

and the cross-sectional area perpendicular to \hat{l} , assuming local cylindrical symmetry about the axis, becomes $\pi R'^2$. We write the initial field as

$$B_l = B_0 f(r/R), \quad B_\theta = qrB_l \tag{16}$$

in which case, the final field becomes

$$B_l = B'_0 f(r'/R'), \quad B'_\theta = q'r'B'_l, \tag{17}$$

where the cylindrical coordinates (r, θ) and (r', θ') are taken in the plane perpendicular to the local axis. (Note the assumption that the field can be written in the same way for both the cylindrical and kinked tubes is violated for the true kink because the internal motion will rearrange the field.)

The axial flux, which is conserved, is

$$\Phi_l = \int_0^R B_l 2\pi r dr = 2B_0 \pi R^2 \int_0^1 f(\zeta)\zeta d\zeta \equiv 2B_0 \pi R^2 I_1, \tag{18}$$

for the initial cylindrical tube, and is

$$\Phi_l = \int_0^{R'} B'_l 2\pi r' dr' = 2B'_0 \pi R'^2 \int_0^1 f(\zeta')\zeta' d\zeta' = 2B'_0 \pi R'^2 I_1, \tag{19}$$

for the final helical tube, where $\zeta \equiv r/R$, and $\zeta' \equiv r'/R'$. We calculate the azimuthal flux as the field perpendicular to the surface extending from $r = 0$ to R along the length of the tube:

$$\Phi_\theta = \int_0^R \int_0^L B_\theta dr dl = B_0 qR^2 L \int_0^1 f(\zeta)\zeta d\zeta = B_0 qR^2 LI_1. \tag{20}$$

The flux through this surface is conserved when the tube kinks, and is

$$\begin{aligned} \Phi_\theta &= \int_0^{R'} \int_0^{L'} B'_\theta dr' dl' = B'_0 q'R'^2 L' \int_0^1 f(\zeta')\zeta' d\zeta' \\ &= B'_0 q'R'^2 LI_1. \end{aligned} \tag{21}$$

The third conserved quantity is the mass M in the tube which, assuming $\rho = \text{constant}$ for this high- β plasma, gives

$$M/\rho = L\pi R^2 = L\pi R'^2. \tag{22}$$

From conservation of axial flux, azimuthal flux, and mass, we find that

$$R'^2 = \frac{R^2}{\kappa}, \quad B'_0 = \kappa B_0, \quad q' = \frac{q}{\kappa}. \tag{23}$$

The writhe of the tube will have an effect on q that is not taken into account here (see Longcope & Klapper 1997 for a discussion of twist and writhe). This effect will be smaller for smaller writhe, or larger wavelength of the kink, so we expect this calculation to fit the actual kink behavior best at small k .

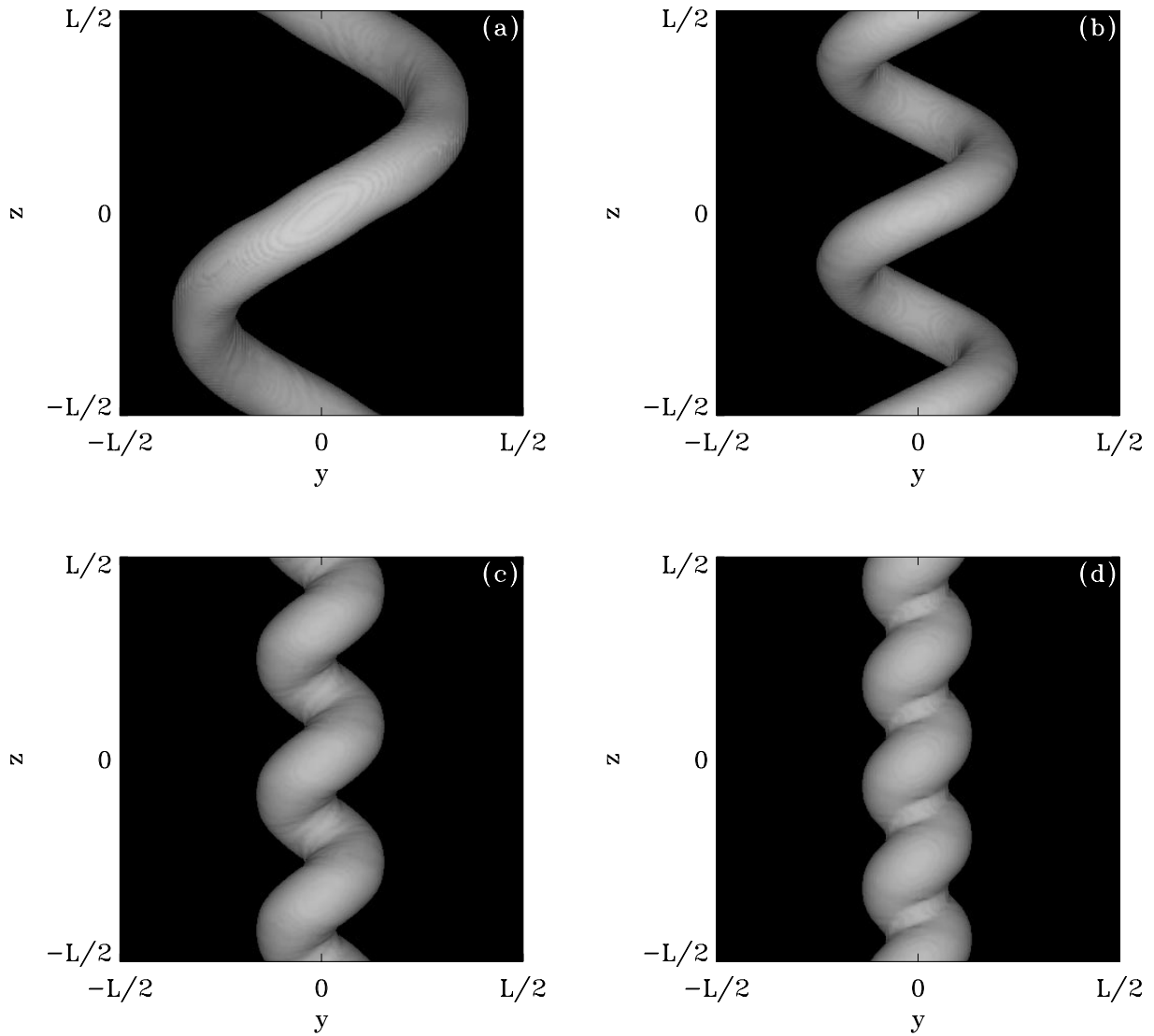


FIG. 2.—Isosurfaces of $|B|^2 = |B|_{\max}^2/6$ for four single-mode kinks with $\alpha = 0.25$ and $qR = 5.89$ (profile D). (a): $n = 1$ kink at $t = 7R/v_A$. (b): $n = 2$ kink at $t = 3R/v_A$. (c): $n = 3$ kink at $t = 8R/v_A$. (d): $n = 4$ kink at $t = 10R/v_A$. Note all but the $n = 1$ kink are in equilibrium at the time shown.

Now we can compare the energy for these two tube configurations: the magnetic energy for the cylindrical tube is

$$\begin{aligned}
 E_B &= \frac{1}{8\pi} \int_0^R \int_0^L 2\pi r dr dl B_0^2 (1 + q^2 r^2) f^2\left(\frac{r}{R}\right) \\
 &= \frac{R^2 L B_0^2}{8} \left[\int_0^1 2f^2(\zeta) \zeta d\zeta + q^2 R^2 \int_0^1 2f^2(\zeta) \zeta^3 d\zeta \right] \\
 &\equiv \frac{R^2 L B_0^2}{8} [I_2 + q^2 R^2 I_3], \tag{24}
 \end{aligned}$$

and when the cylindrical tube evolves to its final helical state, the energy is

$$\begin{aligned}
 E'_B &= \frac{1}{8\pi} \int_0^{R'} \int_0^{L'} 2\pi r' dr' dl' B_0'^2 (1 + q'^2 r'^2) f^2\left(\frac{r'}{R'}\right) \\
 &= \frac{R'^2 L' B_0'^2}{8} \left[\int_0^1 2f^2(\zeta') \zeta' d\zeta' + q'^2 R'^2 \int_0^1 2f^2(\zeta') \zeta'^3 d\zeta' \right] \\
 &= \frac{R'^2 L' B_0'^2}{8} [I_2 + q'^2 R'^2 I_3]. \tag{25}
 \end{aligned}$$

Substituting equations (15) and (23) into equation (25), we find that

$$\frac{E'_B}{E_B} = \frac{\kappa^2 I_2 + q^2 R^2 I_3 / \kappa}{I_2 + q^2 R^2 I_3}. \tag{26}$$

The axial magnetic energy therefore increases quadratically with the extension factor κ , and the azimuthal energy decreases with κ^{-1} . The interplay of these two gives an energy minimum at

$$\kappa = \left(\frac{q^2 R^2 I_3}{2I_2} \right)^{1/3}, \tag{27}$$

therefore giving an optimal displacement Δx for each kink mode with wavenumber k , subject to the constraint that $\kappa \gtrsim 1$, i.e., that $L \gtrsim L$. For the α -profile tubes, the integrals I_2 and I_3 become

$$I_2 = \frac{1}{2\alpha + 1}, \quad I_3 = \frac{1}{(2\alpha + 2)(2\alpha + 1)}. \tag{28}$$

We plot the energy release predicted by equation (26) versus the optimal displacement predicted by equation (27) for the

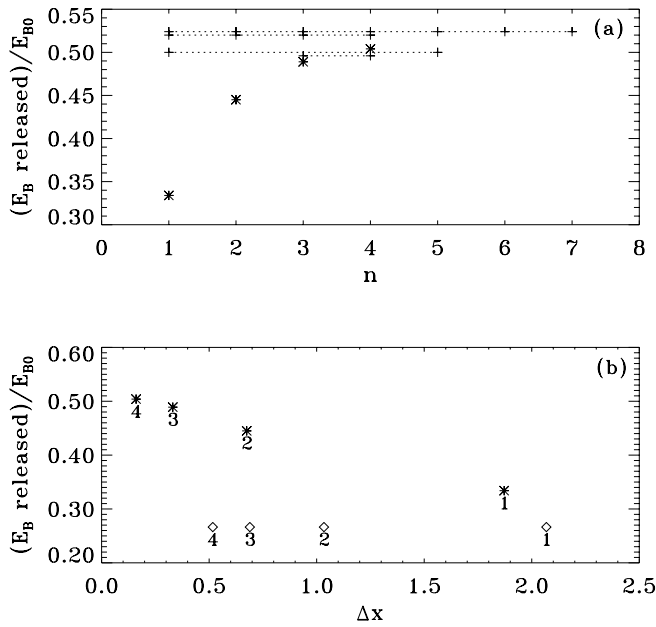


FIG. 3.—Magnetic energy released by the kink ($E_{Bf} - E_{B0}$; see eq. [13]) vs. kink mode n in (a) and vs. Δx , the field weighted displacement of the tube in (b). All are profile D tubes. The asterisks in (a) represent the single-mode kinks. The crosses in (a) connected by dotted lines represent the multiple-mode kinks: a cross marks each mode present in that kink. Note that the $n = 1$ kink simulation appears twice: once while it is only an $n = 1$ kink, not in equilibrium, and once after it has saturated as an $n = 1$ and $n = 5$ multimode kink. The asterisks in (b) show simulation results for the single-mode kinks, and the diamonds show the predicted results for single mode stretching-unstable kinks. Each point in (b) is labeled with its mode number n .

$\alpha = 0.25$, $qR = 5.83$ profile tube at $n = [1, 2, 3, 4]$ as the diamonds in Figure 3b. The asterisks in this figure show the energy release and displacement found for each of these modes from the simulations. The additional effects of writhe and internal motion allow each of the tubes to reach a lower energy kink, at a lower displacement. But these four modes do follow the predicted trend that the displacement increases with decreasing n . In fact, in the low- n limit, as the displacement gets very large, the actual kink behavior approaches that predicted by this analysis, indicating that the writhe and internal motion become less effective at reducing the magnetic energy as the kink wavelength increases.

The above argument gives a critical twist for the kink, namely a twist at which it is energetically favorable for the tube to get longer. The tube length is constrained to be $L \geq L_c$, so $\kappa \geq 1$. Setting $\kappa = 1$ in equation (27), we find a critical twist for this stretching-unstable kink of

$$q_{cr, st} = 2\sqrt{\alpha + 1/R}. \quad (29)$$

This is the same critical twist that Parker (1979, p. 172) finds by arguing that a tube will become kink unstable when the net magnetic tension drops to zero. As this part of the kink decreases the magnetic energy by stretching the tube, it does not depend on the sign of k relative to q . When $q > q_{cr, st}$, positive- k kink modes should become unstable. This explains the appearance of positive- k modes in the linear stability calculation (Fig. 1) when $qR > 2.24$ for $\alpha = 0.25$ tubes. Equation (29) gives $q_{cr, st} R = 2.236$ for these tubes, and so we conclude that the positive k modes in Figure 1 are stretching-unstable kink modes. This stretching-

unstable kink stability limit contrasts with the stability limit for the general kink (i.e., including internal motion and writhe) of $q_{cr} R = \alpha^{1/2}$. Twisted tubes become unstable to stretching-unstable kinks only at significantly higher twist values than that required for a general kink. This agrees with the linear prediction of Linton et al. (1996) (§ 3.1) that weakly twisted tubes ($q^2 \ll R^{-2}$) are stable to solid body kinks, which stretch the tubes, but are unstable to internal kinks, which do not stretch them.

In addition to releasing more magnetic energy, we also find that the kinked tube becomes more force-free as n increases from 1 to 4. To illustrate this, we measure the component of the current perpendicular to and parallel to the magnetic field and take the ratio of the two, which we will call the “global magnetic force parameter” Λ :

$$\Lambda \equiv \frac{\int d^3x |\mathbf{J} \times \mathbf{B}|}{\int d^3x |\mathbf{J} \cdot \mathbf{B}|} = \frac{\int d^3x |\mathbf{J}| |\mathbf{B}| \sin \psi}{\int d^3x |\mathbf{J}| |\mathbf{B}| \cos \psi}, \quad (30)$$

where the integrals are taken over the volume of the tube where $|\mathbf{B}|^2 > |\mathbf{B}|_{\max}^2/6$, and $\psi(x)$ is the angle between \mathbf{B} and \mathbf{J} . As $\psi(x) \rightarrow 0$, $\Lambda \rightarrow 0$, and the tube becomes force free. We plot Λ for these single-mode kinks as the asterisks in Figure 4. This shows that, whereas this ratio was initially 3.51 for these tubes (profile D), it becomes less than 1 for the kinked tubes, varying from just over 0.8 for $n = 1$ to just over 0.2 for $n = 4$. As this is a high- β plasma, small pressure fluctuations (relative to the background pressure) can create pressure gradients that easily balance magnetic forces, but in spite of this, the field becomes more force free. We do not have an explanation for this but note it as an interesting result of the simulation. In summary, we find that all the single-mode kinks studied for this field profile release significant magnetic energy and become much more force free. The higher n , higher growth rate modes develop lower amplitude kinks, release more magnetic energy, and become more force free than lower n , lower growth rate modes. Figure 2 shows that these high n mode tubes, such as $n = 3$ and $n = 4$, have large pitch angles and are tightly wound: a tube with one of these kinks at its apex would therefore create a tilted spot region as it first emerged and would

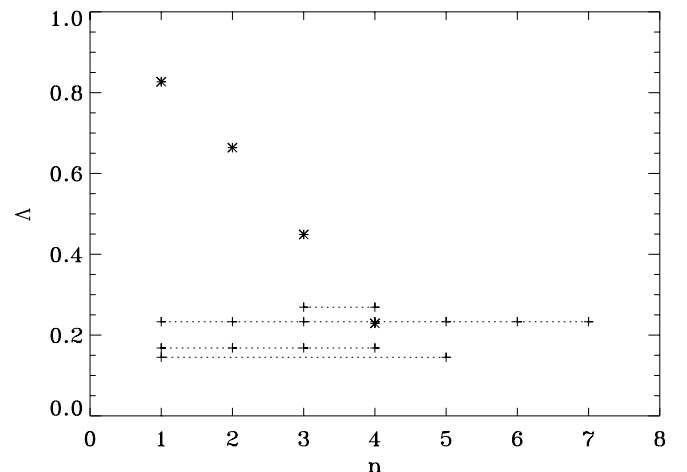


FIG. 4.—Global magnetic force parameter Λ , defined in eq. (30), vs. mode n for profile D tube kinks. The initial value of Λ for a profile D tube is 3.51. As in Fig. 3, the asterisks represent the single-mode kinks, and the crosses connected by dotted lines represent the multiple-mode kinks: a cross marks each mode present in that kink.

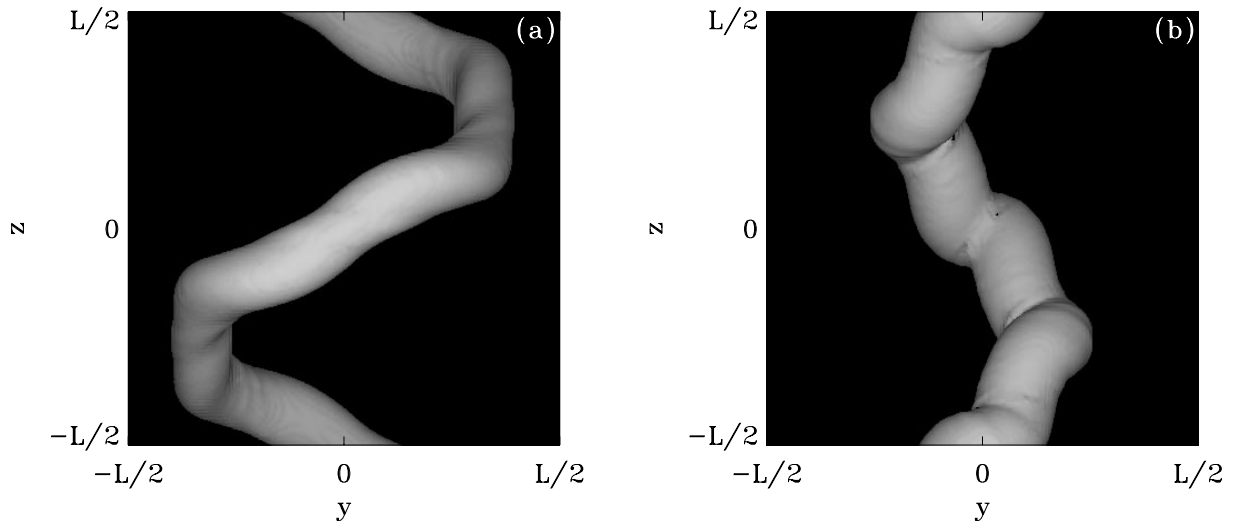


FIG. 5.— $|\mathbf{B}|^2 = |\mathbf{B}|_{\max}^2/6$ isosurfaces of the $n = 1$ kink simulation (a) at $t = 9.6R/v_A$ soon after the $n = 5$ mode has been excited and (b) at $t = 24R/v_A$ after the kinks have saturated.

remain compact and rotate as it emerged further, reproducing several of the observed δ -spot characteristics.

4.2. Multiple-Mode Kinks

Our single-mode kink study is valuable in that it allows us to test our linear predictions and to study how the development of the kink depends on the wavenumber of the excited mode. However, the nonlinear interaction of several simultaneous modes in a kinking tube may produce configurations rather different from those generated by single-mode kinks. As tubes in the convection zone will be constantly buffeted by turbulent convective motions, they will be exposed to a large number of modes and are much more likely to be excited by multiple modes than a single mode. It is thus important to study multimode kinks. In fact, we found in our simulations that even in single-mode kink simulations, additional modes are sometimes excited by either numerical noise or a nonlinear coupling between modes. While the $n = 1$ kink results in a very large amplitude, it does not saturate at a new equilibrium as the higher wavenumber kinks do. Soon after the time step shown in Figure 2a, the $n = 5$ mode begins to affect the evolution of the $n = 1$ kink. An illustration of this mode early in its evolution and a picture of the final equilibrium for the tube, a combination of the two modes, are shown in Figures 5a and 5b, respectively. The $n = 5$ mode significantly decreases the amplitude of the $n = 1$ mode. It also gives the tube a larger pitch, about 90° , and increases the complexity of the tube. The time evolution of the kinetic and magnetic energy of the tube are shown in Figure 6. This shows both the initial peak in the kinetic energy due to the $n = 1$ mode at $t = 6R/v_A$ and the second peak due to the $n = 5$ mode at $t = 12R/v_A$. One can also see how both modes contribute to the decrease in magnetic energy (see discussion below).

We performed a number of simulations wherein several modes are simultaneously excited at the beginning of the simulation (see runs 6–8 in Table 1). To simplify the study of these simultaneously excited kink modes, we again restricted our study to the tube equilibrium given by $qR = 5.89$ and $\alpha = 0.25$ discussed above. In the first simulation, we excited the $n = 3$ and $n = 4$ modes with amplitudes

v_0 and $v_0/2$, respectively. The x and y components of the perturbation velocity on-axis are shown in Figure 7a, from which one can see that the interaction of the modes leads to a beating with the perturbation at a maximum at the midpoint of the tube and decreasing toward the ends. The final kinked state, shown in Figure 8, exhibits a similar beating: the kink is concentrated near the tube midpoint and the ends of the tube are relatively unkinked. This is the major effect of this type of multimode excitation.

How do tubes excited by more complex perturbations evolve? To determine this, we then simulated a four-mode ($n = 1, 2, 3,$ and 4) and a seven-mode (integers $n = 1$ through $n = 7$) kink. For these two simulations, the perturbation amplitude for each mode of wavenumber k was set to $v_0/|k|$. This approximates a turbulent Kolmogorov spectrum for which the amplitude of modes of wavenumber k are proportional to $|k|^{-5/6}$ (see, e.g., Landau & Lifshitz 1987, p. 134). This is the spectrum derived for a neutral fluid, i.e., where the magnetic field is zero, and we argue it is valid here in this high- β environment of the solar convection zone in which the magnetic filling factor is believed to be small.

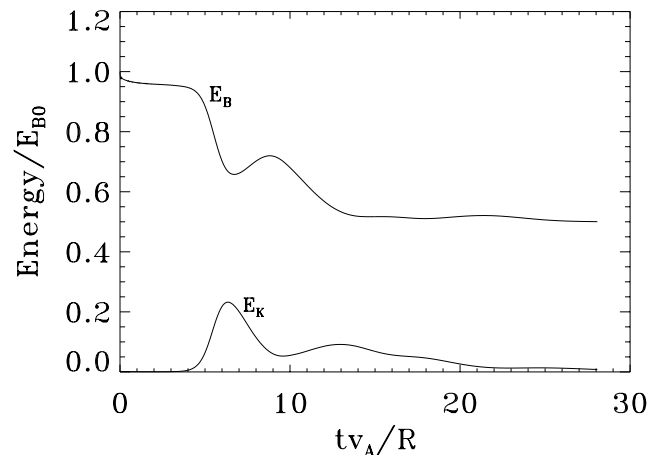


FIG. 6.—Kinetic energy (E_K) and magnetic energy (E_B) vs. time for the $n = 1$ kink simulation. Notice the second peak in the kinetic energy where the $n = 5$ mode is excited.

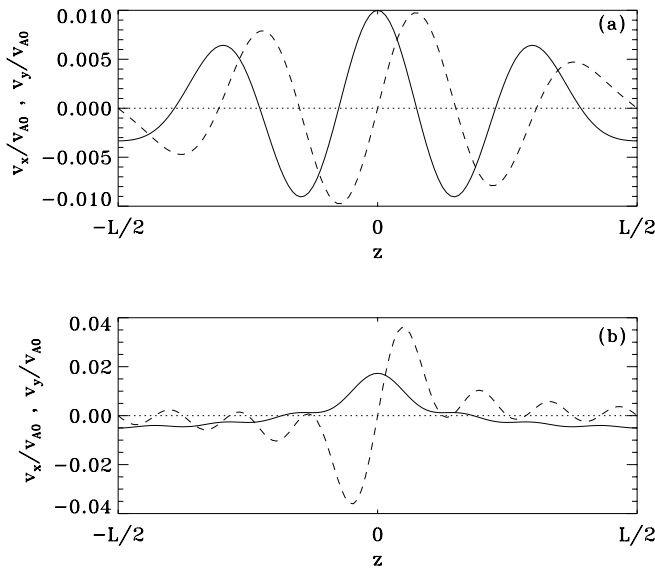


FIG. 7.—Initial velocity perturbation on the tube axis: the solid curve is v_x , and the dashed curve is v_y . (a): The $n=3$ and 4 kink: $v_x = v_0[\cos(6\pi z/L) + \cos(8\pi z/L)/2]$, $v_y = v_0[\sin(6\pi z/L) + \sin(8\pi z/L)/2]$. (b): The seven-mode ($n=1$ to 7) kink: $v_x = v_0 \sum_{n=1}^7 \cos(2\pi n z/L)/n$, $v_y = v_0 \sum_{n=1}^7 \sin(2\pi n z/L)/n$.

(Note it has been argued by Kraichnan that this neutral fluid spectrum should instead be $|k|^{-3/4}$ [see Montgomery 1989, p. 125]). The initial perturbation velocities on-axis for the seven-mode simulation are shown in Figure 7b, from which one can see that the perturbation is highly concentrated near the central cross section of the tube.

We find that the instability proceeds in a very similar fashion in both of these simulations, as illustrated by the nearly identical isosurfaces for the seven-mode simulation in Figure 9b and for the four-mode simulation in Figure 10d. Owing to the interaction of the many modes, these tubes develop a concentrated kink at their midpoint while the rest of the tube remains largely unknicked. The kink near the center of the tube is so violent that the tube folds over on itself and quickly develops a concentrated current sheet

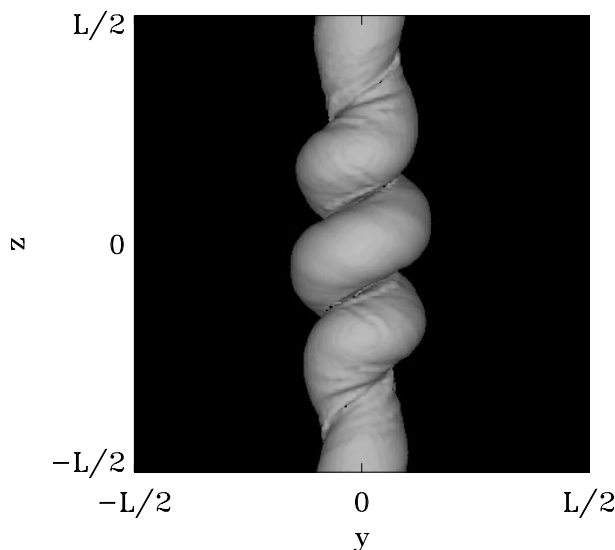


FIG. 8.— $|B|^2 = |B|_{\max}^2/6$ isosurface of the $n=3$ and 4 multimode kink at $t = 7R/v_A$.

near the center of the kink activity, which leads us to infer that two different sections of the tube have come into contact. Figure 9 shows the development of this current sheet and of the tube as the kink evolves. Here isosurfaces of $|B|^2 = |B|_{\max}^2/6$ are plotted in the left-hand half of each panel, while isosurfaces of $|J|^2 = |J|_{\max}^2/3$ are plotted in the right-hand half. In Figure 9a, the kink has just started to form, and the concentration of largest current is at the edge of the tube along its entire length, where the magnetic field drops quickly to zero and the Lorentz force balances the large pressure gradient. In Figure 9b, the kink has already doubled over on itself, and a strong current sheet has developed at the inferred contact point. While the concentrated current at the edge of the tube still exists as before, it now lies below the isosurface threshold value since the magnitude of the current in the new sheet is almost 3 times greater than that in this boundary current. We infer that the new current concentration occurs where the field in one section of the tube, pointing in one direction, has been forced into contact with the field of another section of the tube, pointing in a different direction, resulting in a rapid change in the direction of B over a short distance. In such a configuration, if the resistivity is nonzero, field lines will “break” and “reconnect” to field lines on the opposite side of the current sheet, thus rearranging their topology, and possibly also the morphology of the flux tube. For a discussion of the generation of current sheets and reconnection, see the review by Low (1990) and Chapters 9 and 10 of Parker (1994). Such a release of magnetic stresses through field line reconnection is often cited as the source for coronal flares and the associated reconfiguration of coronal magnetic fields (see, e.g., Manoharan et al. 1996 or the recent review by Tsuneta 1996).

As shown in Figure 9, there is ample evidence from the rapid change of the tube morphology that reconnection is occurring. Figures 9b and 9c show highly distorted, rapidly evolving flux tube isosurfaces and current isosurfaces. By Figure 9d, the tube is evolving more slowly, indicating it is near a new equilibrium configuration, and the current has decreased significantly, though there is still a concentrated sheet at the center of the tube. We also find evidence of reconnection through topological changes of field lines. All field lines were initially helical, winding around the axis a total of 7.5 times over the length of the tube, but as shown by the representative field line traces in Figure 11, field lines near the center of the final tube equilibrium are knotted. The field line shown in Figure 11a has been knotted into a single overhand knot, while the field line shown in Figure 11b has a double overhand knot (Turner & van de Griend 1996). We traced a number of other field lines, starting from $z = -L/2$ at various points along the \hat{y} axis, and found, as shown in Figure 12, that they are singly or doubly knotted near the center of the tube and unknotted near the edge of the tube. The accuracy of these field line trajectories was tested by reducing the step size of the second-order Runge Kutta field line integration (see, e.g., Press et al. 1986, p. 550) until the resulting traces converged. We have not, however, tested them by changing the resolution of the simulations themselves.

The dependence of the kink on the mode or modes excited raises the interesting question of the uniqueness of the final kinked configuration of the tube. Three of the single-mode kinks, $n=2, 3$, and 4, the $n=3$ and 4 two-mode kink, and the $n=1$ mode kink (after the $n=5$ mode

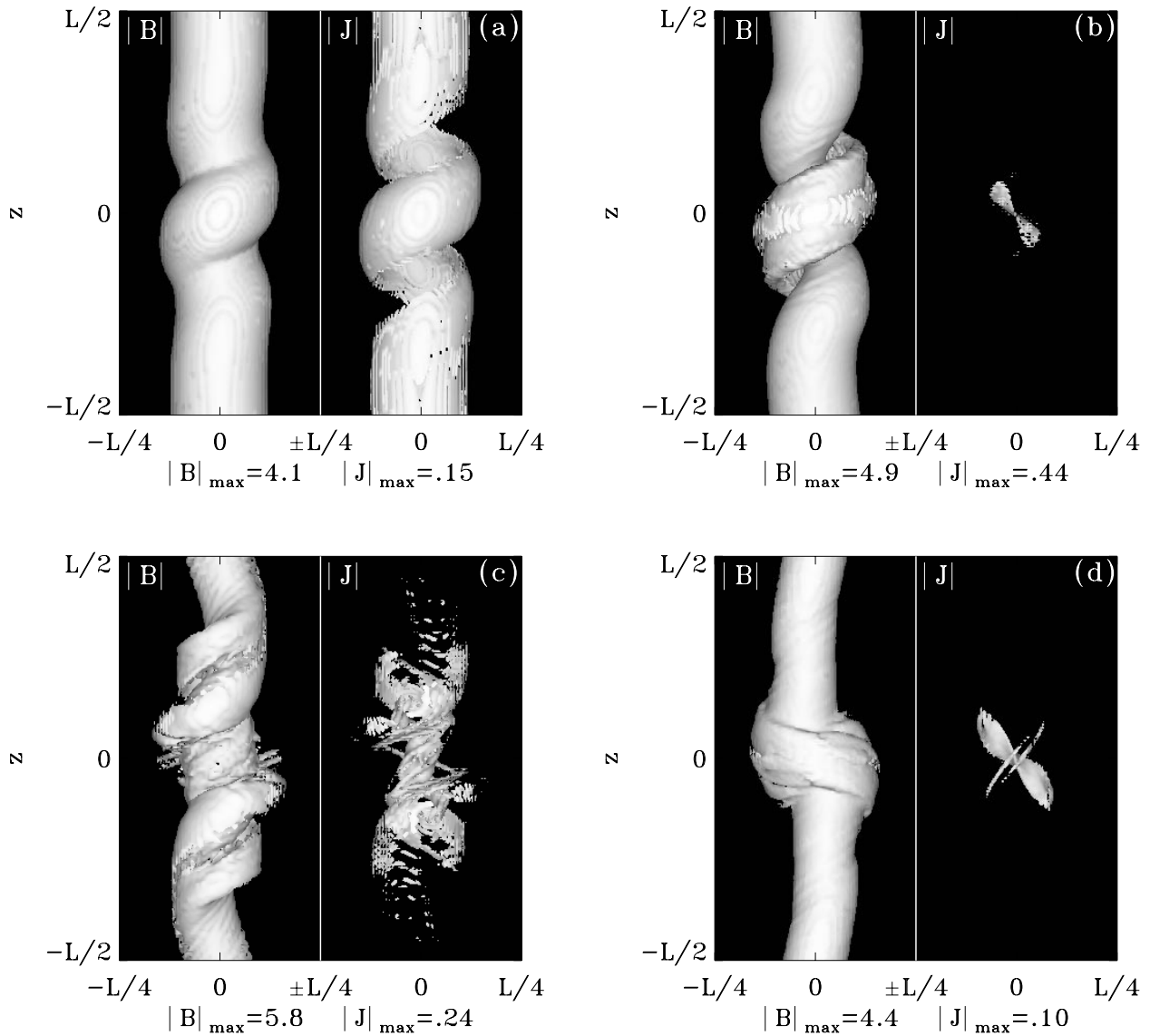


FIG. 9.— $|B|^2 = |B|_{\max}^2/6$ isosurface (left half of each panel) and $|J|^2 = |J|_{\max}^2/3$ isosurface (right half of each panel) for the seven-mode ($n = 1-7$) kink. (a): $t = 2.4R/v_A$, (b): $t = 2.7R/v_A$, (c): $t = 3.4R/v_A$, and (d): $t = 9.8R/v_A$. B is normalized by the initial field strength on axis, B_0 . J is normalized by $cB_0/(4\pi L)$.

has entered and saturated) all appear to reach different equilibrium states, each also different from the seven- or four-mode kink equilibrium. With the exception of the $n = 1$ mode, the initially perturbed kinks therefore seem to have released sufficient magnetic energy that no further kink modes are excited. The magnetic energy loss of the multimode kinks are plotted in Figure 3a with crosses at each mode of the kink connected by a dotted line. This figure shows that almost all simulations mentioned above released about half of the initial magnetic energy of this particular field profile. The $n = 1$ kink released only about 32% and had sufficient free magnetic energy remaining to support an additional unstable mode. The $n = 5$ mode was then excited and released an additional 18% of the initial magnetic energy. The tube then appears to have evolved to a stable equilibrium for which, as in the other stable equilibria, about 50% of the initial magnetic energy has been released. In addition, Figure 4 shows that all of the kinked tubes have evolved to a significantly more force-free state than they were in initially.

These kinks all appear to have evolved to a final state in which about half of the initial magnetic energy has been released and in which they are all at about the same force-free level, as measured by Λ (eq. [30]). Apparently, the initial equilibrium state can evolve to a number of different final states that are each roughly equivalent and locally stable. In the convection zone, however, a kink like the four- or seven-mode kink is more likely to occur, as the tube will constantly be buffeted by turbulent convection zone motions and therefore will be exposed to a large number of unstable modes. As the four- and seven-mode simulations produce very similar results, we argue that they represent the evolution of the tube when a large spectrum of unstable modes is excited. In the next section, we therefore extend our study of the multimode kink, as represented by the four-mode kink.

4.3. Dependence of the Multimode Kink on the Field Profile

As the linear stability of the kink depends on qR and on α , we now explore the nonlinear dependence of the multi-

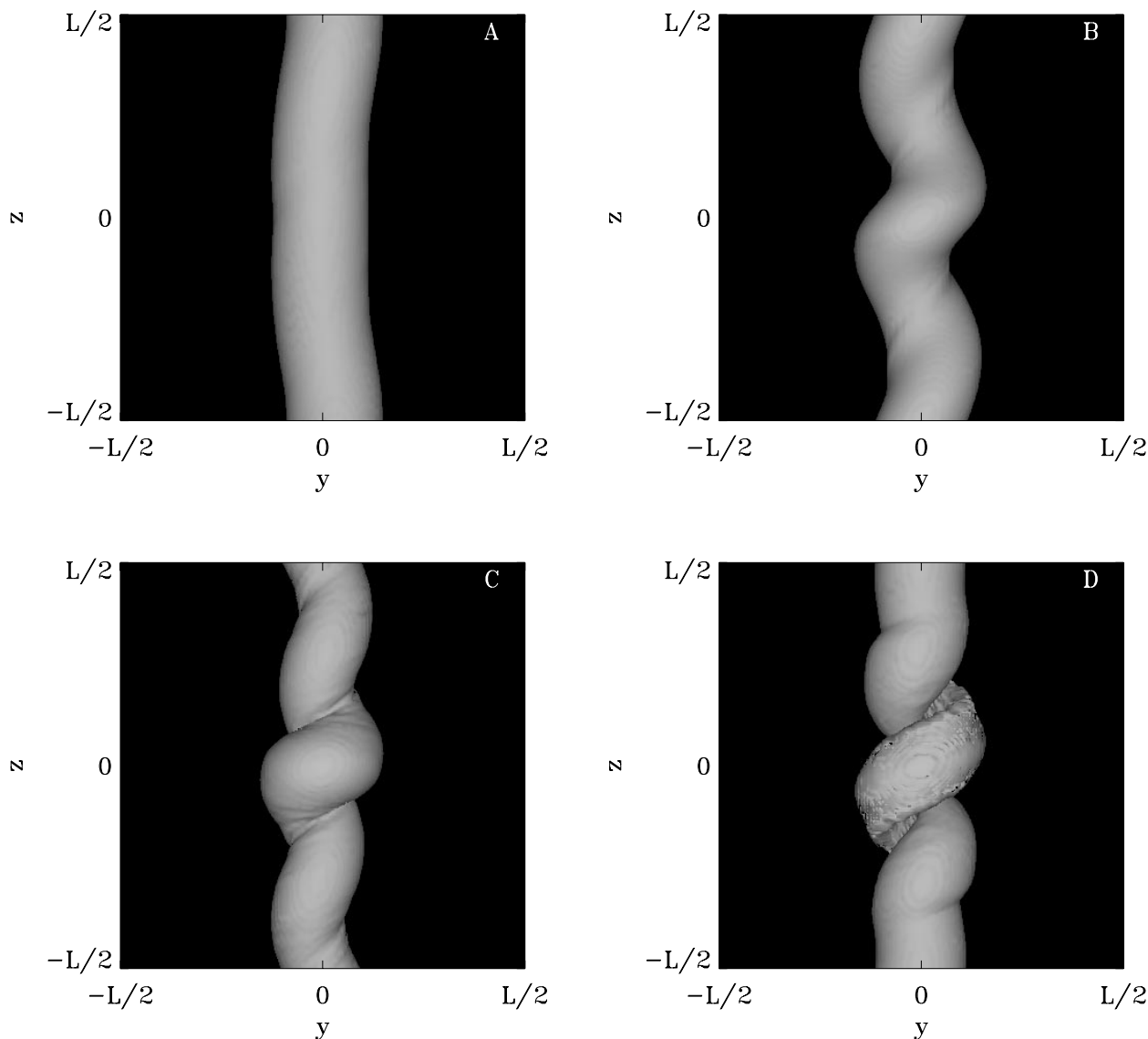


FIG. 10.— $|B|^2 = |B|_{\max}^2/6$ isosurface of four-mode ($n = 1, 2, 3$, and 4) kinks for profiles with $\alpha = 0.25$ and $qR = 1.96$ (a), $qR = 2.95$ (b), $qR = 3.93$ (c), and $qR = 5.89$ (d). The tubes are shown at times $36R/v_A$, $14R/v_A$, $17R/v_A$, and $3R/v_A$, respectively. Note that the tube in panel D has not yet reached an equilibrium state. It continues to evolve much like the kinking tube in Fig. 9.

mode kink on these parameters. The tubes we simulated have $q^2R^2 \gg \alpha$, so we expect variations in qR to have a more significant effect on the kink behavior than variations in α . We therefore concentrate on simulations with varying qR values and perform only one simulation with a different α value. To investigate the multimode kink's dependence on qR , we simulated four different α -profile tubes with $\alpha = 0.25$ and $qR = 1.96, 2.95, 3.93$, and 5.89 , which we denote, respectively, profiles A, B, C, and D (see runs 7 and 9–11 in Table 1). Note that each of these tubes has a ratio R/L of $1/8$. The dispersion relations for these four tubes are shown in Figure 1, from which one can see how qR is predicted to affect the instability, as discussed in § 2. We perturbed each of these tubes with the four modes $n = 1, 2, 3$, and 4 , which are indicated on Figure 1 by the asterisks on each curve, and with amplitudes proportional to $1/n$ as described in § 4.2. Isosurfaces of these tubes after they kink are shown in Figure 10, where all but the profile D tube have saturated. We found that while profile D gives a highly concentrated

kink that leads to reconnection soon after the time shown, as discussed in § 4.2, profile C gives a concentrated kink that is not severe enough to cause reconnection, profile B gives only a weakly concentrated kink, and profile A does not give a concentrated kink. Thus the linear predictions of an increase in instability with qR translate in the nonlinear regime into an increase in the extent of the concentrated kink produced by the interaction of many modes. We interpret this increase in kink extent with increasing qR as representing the increased kinking an unstable tube will experience as it rises through the convection zone and expands with q remaining constant (see § 5).

To test our concentrated kink results on a different tube profile, we then simulated one four-mode kink for $\alpha = 1$ and $qR = 5.89$ (see run 12 in Table 1). This tube's dispersion relation lies between the profile D and profile C curves on Figure 1, and one would therefore expect the kink to be intermediate in extent between that of the profile D and profile C tube kinks. The final equilibrium of this kinked

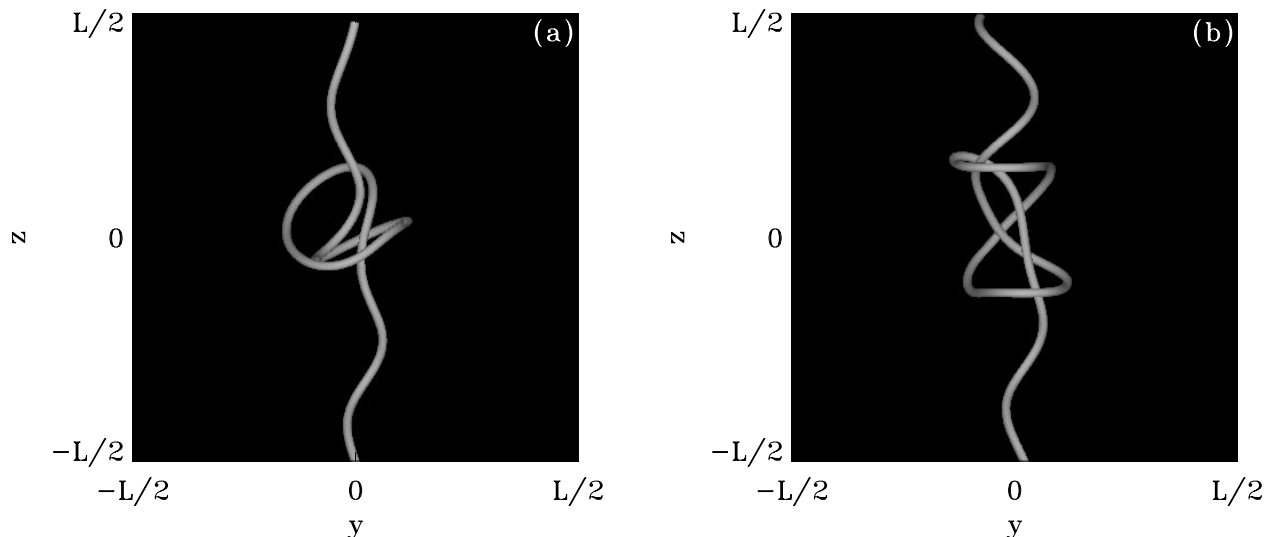


FIG. 11.—Representative magnetic field lines from the final state of the seven-mode kink (Fig. 9d). The traces shown are field lines initiating at (a): $x = 0$, $y = 0$, and $z = -L/2$ and (b): $x = 0.19R$, $y = 0$, and $z = -L/2$. These field lines were initially helical (see Fig. 2 of Linton et al. 1998)

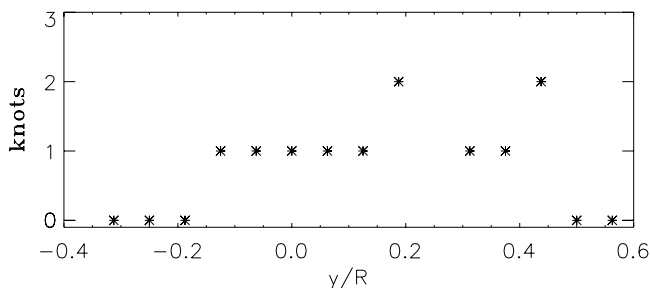


FIG. 12.—Number of knots in field lines traced from points along the y -axis at $z = -L/2$. Doubly knotted field lines look like the field line of Fig. 11b (double overhand), while singly knotted field lines look like the field line in Fig. 11a (overhand).

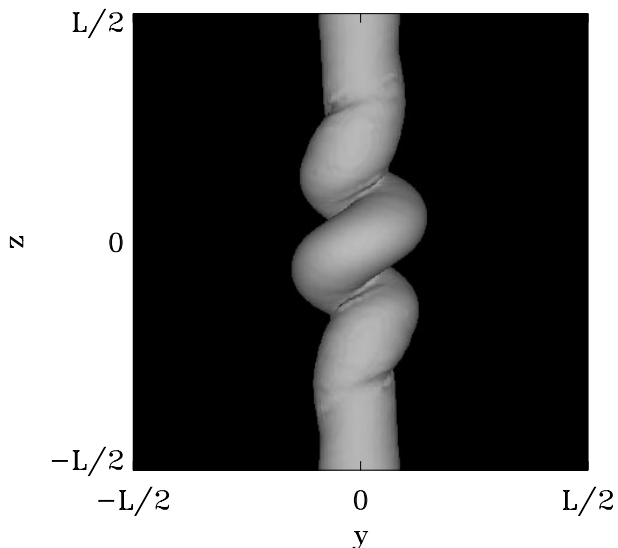


FIG. 13.— $|\mathbf{B}|^2 = |\mathbf{B}|_{\max}^2/6$ isosurface of a four-mode ($n = 1, 2, 3$, and 4) kink for an $\alpha = 1$, $qR = 5.89$ profile. $t = 8R/v_A$.

tube is shown in Figure 13. This tube shows the same characteristic concentrated kink shape as those shown in Figure 10. It has not kinked enough to reconnect as the profile D tube does, but it is more severely kinked than the profile C tube.

As the periodicity of our code does not allow us to include gravity, we cannot simulate the effect of hydrodynamical forces acting on a kinking tube as it rises. It has been shown by Moreno-Insertis & Emonet (1996) and Fan, Zweibel, & Lantz (1998a) that a tube with sufficient twist will remain intact as it rises but will not remain cylindrically symmetric. Rather, the twist concentrates in the upper part of the tube cross section. A comparison of our results with the kink simulations of Fan et al. (1999), however, shows that this does not significantly affect the evolution of the kink instability. In their paper, they studied several isolated, kinking flux tubes rising in a gravitationally stratified atmosphere. The most kink unstable tube profile in their simulations is initially close to our $\alpha = 1$ and $qR = 5.89$ tube, although slightly less twisted ($qR = 4$) and therefore less unstable. Early in its evolution, this tube, shown in Figure 5 of Fan et al., evolves to a state much like that of our $\alpha = 1$ and $qR = 5.89$ tube, shown in Figure 13. However, as the tube in Fan et al.'s simulation expands and becomes more unstable as it rises into fluid of lower density, it evolves into a buckled shape. This buckling is different from the evolution of our profile D tube, which is initially significantly more kink unstable and evolves into a knotted configuration owing to reconnection. This difference is mainly due to the presence of up-down asymmetry produced by the buoyancy and stratification in Fan et al.'s code and to the slow evolution of their tube to a highly unstable state, which we discuss further in the next section.

5. RISE OF A KINKING CONVECTION ZONE FLUX TUBE

Based on this nonlinear study of the kink instability and our linear stability predictions from Linton et al. (1996), we propose the following scenario for the development of a

kink-unstable flux tube as it rises through the convection zone. We do not address the issues of magnetic field generation by the solar dynamo or the creation of a flux tube from the dynamo source region near the base of the convection zone. Rather we start from the point at which a twisted flux tube has broken off from that region and starts to rise toward the solar surface. We do not know in what way the flux tube has gained its twist or what profile the twist in the tube has taken. However, we argue in § 2 that a uniform-twist flux tube is representative of twisted solar flux tubes for the purposes of the kink instability.

A magnetic flux tube is unstable to the external kink only when its twist (q) is greater than the critical twist (q_{cr}) for that tube. For example, consider a flux tube at the base of the convection zone with an α -profile magnetic field (eq. [3]) with $\alpha = 0.25$. The critical twist for this profile is $q_{cr} = \alpha^{1/2}/R = 0.5/R$, so any tube with $qR < 0.5$ will be stable and will not kink. However, as the apex of the tube rises, both q and α will remain constant if the rising portion of the tube expands homologously, so $q_{cr}R$ remains constant as R increases, and the critical twist decreases. If we take the twist in our example tube to be $q = 0.5/R$ at the base of the convection zone, the tube will initially be marginally stable but will become kink unstable soon after it begins to rise and expand. This explains the simulations of Fan et al. (1999): their gravitationally stratified simulation box is deep enough to allow a tube to expand by about a factor of 3 before it has risen to the top. They find that tubes at the base of the simulation box need to have twist greater than half the critical value to become unstable and go through at least one e -folding of the instability before they near the top of the simulation box. Hence, a flux tube that initially has $q = 0.5q_{cr}$ does not exhibit kinking before it reaches the top of the box, while a flux tube with $q = 0.9q_{cr}$ does exhibit kinking, albeit very slight, as it nears the upper boundary (see Fig. 4 of Fan et al. 1999).

Once the tube has expanded enough for the critical twist to be negligible compared to the actual twist, equation (2) predicts that the normalized growth rate will scale as R^2 , and thus expansion will continue to increase the tube's instability. This does not mean the kink will evolve faster: v_A will scale as $1/R$, so the growth rate an external observer sees will not increase. Rather, it means the instability the tube experiences will become more severe, and the final state of tube will be more significantly kinked. Figure 10 shows how this increased instability affects the kink evolution: the four-mode kink gets increasingly severe as qR is increased from profile A to profile D. Finally, it undergoes such a violent kink that it folds over and reconnects. As an example, we consider a marginally stable tube with $qR = 0.5$ and $\alpha = 0.25$ and trace its evolution as it rises and expands. Once the apex of the tube has risen enough to expand by about a factor of 4 it will be the equivalent of tube A in Figure 10. It will be continually buffeted by convection zone motions and will therefore be exposed to a large range of kink modes. For positive twist tubes, negative- k kink modes will be unstable and will therefore be excited but will result in mostly internal motion, as the twist is not yet large enough to give large-amplitude kinks (see tube A in Fig. 10). By the time the apex has expanded by a factor of 6, it is equivalent to profile B, and so larger amplitude kinks can form, and a concentrated kink begins to develop. At this point, positive- k modes also become unstable, but as the negative- k modes are already well developed, we argue that

they will dominate. This is important because the sign of the kink will be observable as the sense of tilt and subsequent rotation of the spot region when the tube emerges, as we discuss in § 6. As we follow the evolution, the tube evolves to a kink as for profile C when it has expanded by a factor of 8 and develops a kink severe enough to cause reconnection, as for profile D, by the time it expands by a factor of 12. The density decreases by about 6 orders of magnitude from the base of the convection zone to the photosphere, so a rough estimate, based on mass conservation within the tube, gives a radial expansion factor of 100. This indicates that a radial expansion factor of at least 12 as a tube rises to the surface is reasonable, and thus a tube that was initially marginally stable could produce a concentrated kink and a current sheet during its rise to the photosphere.

The results of Fan et al. (1999), however, do provide a cautionary note for this scenario. Their most unstable tube (illustrated in Fig. 5 of that paper) evolves to a buckled tube with the axis tilted by about 120° . Our profile D tube, in contrast, reconnects before its axis tilts by 90° . The tube in Fan et al. is initially significantly less kink unstable than our profile D tube, and the kink instability is enhanced slowly as the tube rises and expands in the stratified fluid. Therefore, that tube kinks more gradually, while our profile D tube starts off in a very unstable state and can kink violently and rapidly evolve a current sheet. We expect, however, that a rising tube will eventually develop a current sheet as seen in Figure 10*d*. While the slow evolution of the kink will postpone the formation of this current sheet, as the tube rises it will eventually expand sufficiently that the buckling will force one section of the tube into another, and the current sheet will form.

Whether a kinked tube, having evolved to a state with a large current sheet at the juxtaposition of two differently directed magnetic fields, would undergo significant reconnection in the convection zone is a difficult question: the resistivity is very low in the convection zone, so while reconnection will occur, one might expect it to be very slow. Since we cannot observe flux tubes in the convection zone, we cannot test this prediction. On the other hand, many observations from *Yohkoh* (see, e.g., Manoharan et al. 1996 and Tsuneta 1996) have shown that the configuration of the coronal magnetic field can change quite rapidly during flares, so it is apparent that reconnection does occur in the corona, perhaps driven by an enhanced resistivity due to anomalous plasma processes (see, e.g., Priest 1982, p. 79) or the development of turbulence in the current sheets where reconnection occurs (see, e.g., Dahlburg, Antiochos, & Zang 1992). Therefore, if a kink like that of tube D were to be achieved in the convection zone, it may not reconnect as it did in our simulation (owing to the relatively high resistivity in our code compared to that in the convection zone), but it could reconnect after it emerged.

This indicates a key connection with the high flare activity of δ -spots. While reconnection of magnetic fields is the likely source of flare activity, and the local magnetic configuration that leads to current sheets and reconnection has been well studied (see, e.g., Low 1990 and Parker 1994), it not well known how the large-scale coronal fields develop into a configuration that is conducive to reconnection. What we have shown here is that a highly twisted tube can develop a concentrated kink configuration that undergoes significant reconnection. Therefore, if such a concentrated kink were the cause of δ -spot regions, this would provide a

promising explanation for the high flare activity of these regions.

6. CONCLUSIONS

The real test of the relationship between the concentrated kink we have studied and δ -spot active regions is in the emergence of the kink through the photosphere, where the simulations can be compared with photospheric observations. As the concentrated kink at the apex of the flux tube emerges through the photosphere, it creates a “spot group” that evolves as shown in Figure 14. This figure shows the magnetic field on four surfaces intersecting the final state of the profile D tube. As the tube will be arched in the convection zone, but is initially straight in our simulation, we take curved surfaces through the tube, as shown in Figure 15, to represent the flat photosphere intersecting an arched tube. Note that the surface is curved in the x - z plane

and is parallel to the \hat{y} axis. The gray scale in Figure 14 is the magnetic field perpendicular to the intersecting surface, with white (black) representing positive (negative) field. The field in the plane of the surface is represented by the vectors.

The active region first emerges, in Figure 14a, with a clockwise tilt between the opposite polarity regions of about 120° away from the usual Hale-Nicholson orientation. It then rotates counterclockwise in the next three panels until it is approximately oriented in the Hale-Nicholson orientation. Note the sense of tilt and rotation depends on the handedness of the kink: a right-handed kink ($k < 0$), which occurs for right-hand twisted tubes ($q > 0$), will emerge with an initial clockwise tilt, followed by counterclockwise rotation, and the inverse will occur for left-hand twisted, left-hand kinked tubes. During its rotation, in Figures 14b and 14c, the region develops significant shear along its neutral line. This is due not to photospheric

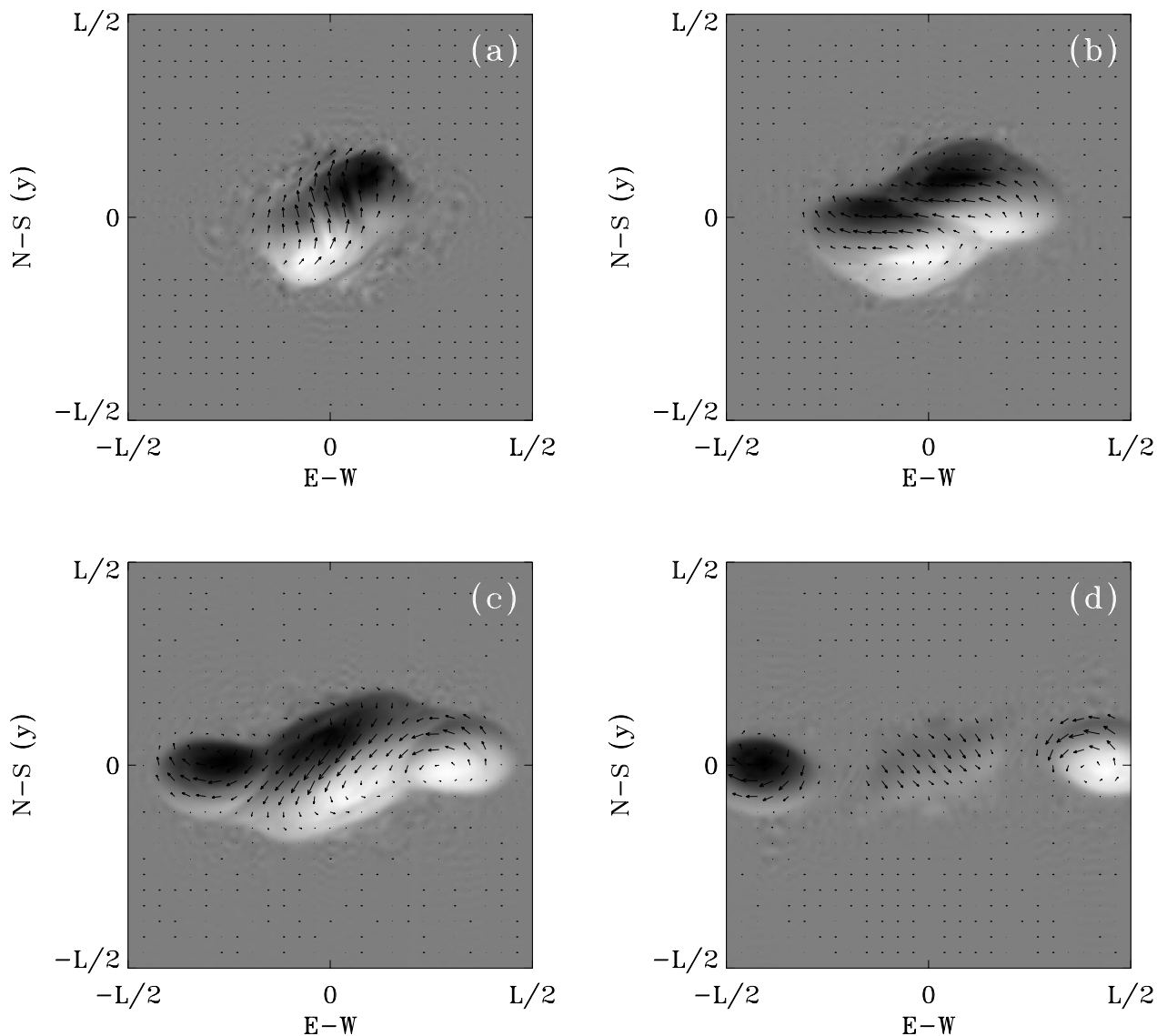


FIG. 14.—Vector magnetogram of the spot region that would result from the emergence through the photosphere of the kinked flux tube pictured in Fig. 15. Each panel corresponds to the surface marked with the same letter in Fig. 15. The gray scale shows the magnetic field perpendicular to the surface: positive (negative) field is white (black). The vectors show the magnetic field lying on the surface. The region emerges highly tilted away from the east-west direction in (a), rotates and develops strong shear along the magnetic neutral line while remaining compact in (b) and (c), and separates into two opposite polarity regions in (d).

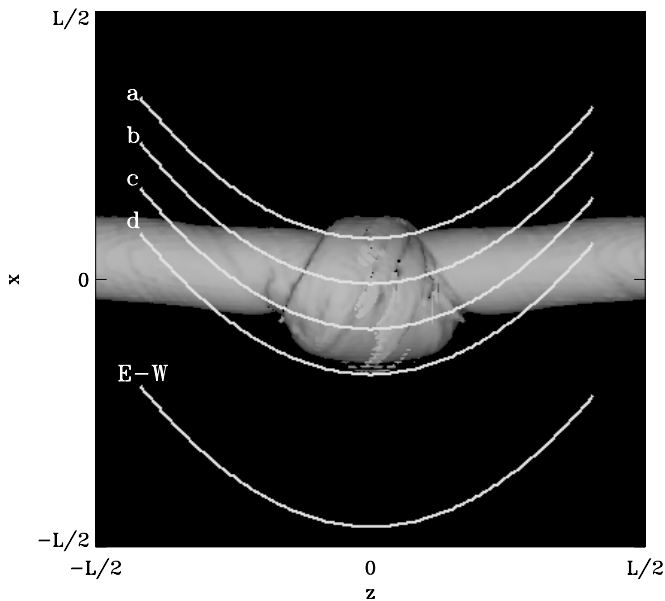


FIG. 15.— $|B|^2 = |B|^2_{\max}/6$ isosurface of the seven-mode tube, shown from an angle rotated by 90° about the \hat{x} axis relative to the view given in Fig. 9d. The lines superimposed on the figure show the curved surfaces intersecting the tube. These curved surfaces intersecting the unarched tube represent a flat photosphere intersecting an arched tube. The field on each of these planes is shown in Fig. 14. The line marked “E-W” shows the east-west direction.

motions but rather to the magnetic field configuration in the tube. Finally it remains compact during its rotation and during the development of its shear. The opposite polarity spots only separate once the concentrated kink has fully emerged. We expect the reconnection and any associated flare activity will occur during this initial emergence, as the concentrated kink expands into the corona.

While Leka et al. (1996) have shown that photospheric motions are not responsible for this observed flux tube rotation and shear, there remains the possibility that turbulent convection zone motions, rather than the kink instability, could be responsible for this. In fact Fisher, Fan, & Howard (1995) concluded that there is an observable effect of convective motions on active regions. While the average tilt angle of active regions away from the Hale orientation is small, there is a measurable dispersion of tilts about the average value. This dispersion is likely due to the buffeting of rising flux tubes by convection zone motions. Fisher et al. (1995) studied this dispersion in tilt angles and found that small active regions display a dispersion of $\sim 30^\circ$ about the average tilt angle. However, they found that this dispersion decreases for larger active regions to about 6° . As flare-productive δ -spot active regions associated with strong flares are usually quite large, this indicates that convective motions should have little effect on the flux tubes that create these δ -spots. One can check this prediction by comparing the sense of tilt and rotation of δ -spots with the sign of their twist. As discussed above, the kink results in a correlation between these two. On the other hand, convective motions would not lead to such a correlation, as discussed in Linton et al. (1998). A statistical study of δ -spots should therefore be able to determine which of these two possible mechanisms is responsible for creating δ -spot flux tubes.

We find, therefore, that the emergence of the concentrated kink displays all the features we have identified as

characteristic of δ -spots. An additional feature of this scenario is that we find the opposite polarity spots will eventually separate if the tube continues to emerge and no additional kinks have formed beyond the concentrated kink at the apex. As reconnection will occur during the tube's emergence, the tube could be largely reconfigured by the time it reached this stage and may no longer resemble the tube in Figure 15. If the tube does keep its integrity, however, the opposite polarity spots will eventually separate after the concentrated kink emerges fully. In fact, Lites et al. (1995) find a very similar behavior to our concentrated kink emergence in their study of a δ -spot active region. They see a compact δ -spot group emerge and exhibit strong left-handed twist and strong shear along its neutral line. (Note that it emerges with a clockwise rotation, in contrast to our analysis, which predicts an initial counterclockwise rotation.) At the end of the evolution, the δ -spot disappears, leaving a twisted loop system visible in X-rays in the corona and two separated pores of opposite polarity in the photosphere. These two pores could be what remains of the twisted flux tube after the concentrated kink has emerged and reconnected, as in Figure 14d, while the coronal loop system could be the emerged concentrated kink. Such evidence of separated bipolar spots is not usually associated with δ -spot region behavior. In fact, Lites et al.'s interpretation of this observation is that the twisted flux region has emerged completely and is no longer connected to the convection zone at the end of the observation. It is difficult from this observation to tell which of these interpretations is more accurate, so this issue warrants a detailed observational study of δ -spots to discover if indeed there is any evidence that a fully emerged δ -spot region is still tied to the convection zone in such a way.

In summary, we studied the current-driven kink instability in twisted flux tubes as a mechanism for the formation of δ -spot active regions. We found that, when perturbed with a single unstable mode, the tubes develop kinks that saturate at finite amplitude. The simultaneous excitation of a number of unstable modes produces concentrated kinks that display large tilt angles and produce compact kinks at the tube midpoint, thus creating a tube with the required morphology for δ -spot formation. Such a kinked tube would emerge highly tilted away from the Hale-Nicholson configuration and would rotate, develop strong magnetic shear along the neutral line, and remain compact as it evolved. A very kink-unstable tube will kink to the point at which it folds over on itself and creates a current sheet at which the magnetic field reconnects. This changes the morphology of both the tube and its field lines and could be the source of the flare activity in δ -spots. In addition to these characteristics of the tube emergence, which agree with observed δ -spot characteristics, our simulations predict that the sense of the initial tilt (relative to the Hale orientation) will be clockwise (counterclockwise) for a tube with right- (left-) handed twist, the subsequent rotation will be counterclockwise (clockwise) and the region will separate into two isolated spots after the concentrated kink has fully emerged. In the future we plan to study a large number of δ -spot regions and compare their evolution with these predictions.

We wish to thank Suzanne Hawley and Dana Longcope for useful discussion and comments. This work was supported by NASA GSRP training grant NGT-51377, the NASA High Performance Computing and Communica-

tions Program, NSF grants AST 95-28474 and AST 95-21779, NASA grant NAG 5-4181, and the NASA Space Physics Theory Program. The numerical simulations were

performed on the NRL CM5-E under a grant of time from the DoD HPC program.

REFERENCES

- Alfvén, H. 1950, *Tellus*, 2, 74
 Aydemir, A., Wiley, J., & Ross, D. 1989, *Phys. Fluids B*, 1, 774
 Baty, H. 1997, *A&A*, 318, 621
 Dahlburg, R., Antiochos, S., & Norton, D. 1997, *Phys. Rev. E*, 56, 2094
 Dahlburg, R., Antiochos, S., & Zang, T. 1992, *Phys. Fluids B*, 4, 3902
 Fan, Y., Zweibel, E., & Lantz, S. R. 1998a, *ApJ*, 493, 480
 Fan, Y., Zweibel, E., Linton, M., & Fisher, G. 1998b, *ApJ*, 505, L59
 ———, 1999, *ApJ*, 521, 460
 Fisher, G. H., Fan, Y., & Howard, R. F. 1995, *ApJ*, 438, 463
 Galsgaard, K., & Nordlund, A. 1997, *J. Geophys. Res.*, 102, 219
 Gilman, P., & Glatzmaier, G. 1981, *ApJS*, 45, 335
 Hale, G. E., Ellerman, F., Nicholson, S. B., & Joy, A. H. 1919, *ApJ*, 49, 153
 Kruskal, M. D., & Schwarzschild, M. 1958, *Proc. R. Soc. London A*, 223, 348
 Künzel, H. 1960, *Astron. Nachr.*, 285, 271
 Landau, L. D., & Lifshitz, E. M. 1987, *Fluid Mechanics* (Oxford: Butterworth-Heinemann)
 Leka, K., Canfield, R., McClymont, A., & van Driel Gesztelyi, L. 1996, *ApJ*, 462, 547
 Linton, M. G., Dahlburg, R. B., Longcope, D. W., & Fisher, G. H. 1998, *ApJ*, 507, 404
 Linton, M. G., Fisher, G. H., Dahlburg, R. B., Fan, Y., & Longcope, D. W. 1999, *Adv. Space Res.*, in press
 Linton, M. G., Longcope, D. W., & Fisher, G. H. 1996, *ApJ*, 469, 954
 Lionello, R., Velli, M., Einaudi, G., & Mikic, Z. 1998, *ApJ*, 494, 840
 Lites, B. W., Low, B. C., Pillet, V. M., Seagraves, P., Skumanich, A., Frank, Z. A., Shine, R. A., & Tsuneta, S. 1995, *ApJ*, 446, 887
 Longcope, D. W., & Klapper, I. 1997, *ApJ*, 488, 443
 Low, B. C. 1990, *ARA&A*, 28, 491
 Manoharan, P., van Driel-Gesztelyi, L., Pick, M., & Demoulin, P. 1996, *ApJ*, 468, L73
 Matsumoto, R., Tajima, T., Chou, W., Okubo, A., & Shibata, K. 1998, *ApJ*, 493, L43
 Moffatt, H., & Ricca, R. 1992, *Proc. R. Soc. London A*, 439, 411
 Montgomery, D. 1989, in *Lecture Notes on Turbulence*, ed. J. R. Herring & J. C. McWilliams (Singapore: World Scientific), 75
 Moreno-Insertis, F., & Emonet, T. 1996, *ApJ*, 472, L53
 Parker, E. N. 1979, *Cosmical Magnetic Fields, Their Origin and Their Activity* (Oxford: Clarendon Press)
 ———. 1994, *Spontaneous Current Sheets in Magnetic Fields* (Oxford: Oxford Univ. Press)
 Press, W. H., Flannery, B. P., Teukolsky, S. A., & Vetterling, W. T. 1986, *Numerical Recipes: The Art of Scientific Computing* (Cambridge: Cambridge Univ. Press)
 Priest, E. R. 1982, *Solar Magnetohydrodynamics* (Boston: Reidel)
 Sammis, I. R., & Zirin, H. 1998, paper given at American Geophysical Union, Spring Meeting, SH22A, 4
 Shafranov, V. D. 1957, *J. Nucl. Energy II*, 5, 86
 Stix, M. 1989, *The Sun, An Introduction* (New York: Springer)
 Suydam, B. R. 1959, in *Proc. 2nd UN Internat. Conf. Peaceful Uses of Atomic Energy*, 31, 157
 Sykes, A., & Wesson, J. A. 1976, *Phys. Rev. Lett.*, 37, 140
 Tanaka, K. 1980, in *Solar-Terrestrial Predictions Proc.*, ed. R. Donnelly, 3 (NOAA-ERL), C1
 ———. 1991, *Sol. Phys.*, 136, 133
 Tsuneta, S. 1996, in *ASP Conf. Ser. 111, Magnetic Reconnection in the Solar Atmosphere*, ed. R. D. Bentley & J. T. Mariska (San Francisco: ASP), 409
 Turner, J. C., & van de Griend, P. 1996, *History and Science of Knots* (Singapore: World Scientific)
 Vlad, G., & Bondeson, A. 1989, *Nucl. Fusion*, 29, 1139
 Waddell, B. V., Rosenbluth, M. N., Monticello, D. A., & White, R. B. 1976, *Nucl. Fusion*, 16, 528
 Zirin, H., & Liggett, M. A. 1987, *Sol. Phys.*, 113, 267